PORPHYRIN-POLYMER SUPRAMOLECULAR ASSEMBLIES IN WATER: SPECTROSCOPIC AND THERMODYNAMIC PROPERTIES

by

Barrington J. Hwang

Submitted in partial fulfillment of the

requirements for Departmental Honors in

the Department of Chemistry

Texas Christian University

Fort Worth, Texas

May 2, 2014

PORPHYRIN-POLYMER SUPRAMOLECULAR ASSEMBLIES IN WATER:

SPECTROSCOPIC AND THERMODYNAMIC PROPERTIES

Project Approved:

Supervising Professor: Onofrio Annunziata, Ph.D.

Department of Chemistry

David Minter, Ph.D.

Department of Chemistry

Matthew Chumchal, Ph.D.

Department of Biology

ABSTRACT

Porphyrins are molecules that are investigated for their importance in applications such as cancer therapy, photochemical processes, and chemical catalysis. One important porphyrin property is the ability to absorb visible and ultraviolet light when illuminated. This leads to a transfer of energy from the excited porphyrin molecule to nearby oxygen molecules. The resulting excited oxygen molecules are toxic to tumor cells and infectious bacteria. Interestingly, porphyrins are known to self-aggregate in water. This property affects porphyrin light-absorbance behavior and therefore impacts the applications of these molecules. Thus, it is important to identify those factors that modulate porphyrin self-aggregation.

Here, we have investigated the effect of the polymer polyvinylpyrrolidone (PVP) on the spectrophotometric behavior of tetraanionic meso-tetrakis(4-sulfonatophenyl)porphyrin (TPPS). It is known that TPPS self-aggregation significantly increases from neutral to acidic pH. Thus, our experiments were performed at pH 3.0, 4.5 and 7.0. In all cases, our measurements showed that TPPS binds to PVP. Furthermore, contrary to the case of free porphyrin, our results demonstrated that the spectrophotometric properties of porphyrin-polymer supramolecular assemblies are independent of pH. To characterize strength and stoichiometry of the resulting porphyrin-polymer supramolecular assemblies, we performed isothermal-titration-calorimetry (ITC) measurements at neutral pH. This technique allowed us to identify the correct model describing the complicated associative equilibria occurring in solution. Furthermore, our ITC results revealed that the formation of porphyrin-polymer supramolecular assemblies is entropically favored with respect to porphyrin self-aggregation.

ACKNOWLEDGEMENTS

I would like to thank Professor Onofrio Annunziata and Viviana Costa for assisting and guiding me on this project. This work was supported by the NSF RI grant (CHE-1126710), TCU Research and Creative Activity Funds and TCU SERC. Additionally, the material in this thesis is also presented in a paper recently accepted for publication (see reference below).

V.C.P. da Costa, B.J. Hwang, S.E. Eggen, M.J. Wallace and O. Annunziata, "Formation and thermodynamic stability of polymer-porphyrin supramolecular structures in aqueous solutions", *J. Chem. Thermodynamics*, in press.

TABLE OF CONTENTS

LIST OF FIGURES

LIST OF TABLES

INTRODUCTION

Porphyrins are organic, disk-shaped aromatic molecules with a central cavity (Fig. 1). These molecules have four pyrrole rings connected by single and double carbon bonds. Pyrrole rings consist of four carbon atoms and one nitrogen atom arranged in a five-membered ring. These tetrapyrollic molecules are known in chemistry and biology for their pharmaceutical[1], photochemical[2], supramolecular assembly[3], catalytic[4,5], and optical applications[6]. Porphyrins can be artificially or naturally produced. In humans, porphyrins are naturally produced in the heme pathway when synthesizing hemoglobin, in myoglobin production, and in the cytochrome pathways. In plants, chlorophyll production involves molecules similar to porphyrins.[7]

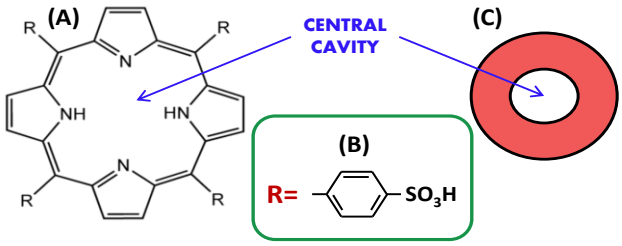

Figure 1 – **(A)** General chemical structure of a porphyrin. The peripheral R groups are generic chemical groups. **(B)** Peripheral chemical groups of the specific porphyrin, meso-Tetrakis(4-sulfonatophenyl)porphyrin, considered in this project. **(C)** The porphyrin structure may be roughly described as a disk with a central circular cavity.

The central cavity of porphyrins allows for the insertion of other particles such as metal ions (e.g. iron) (Fig. 2). This associative process does not significantly affect porphyrin structural properties. In addition, the conjugated electron system and aromaticity play a role in stabilizing the structure.

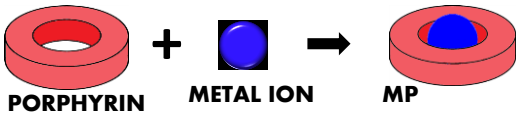

Figure 2 – The association between a porphyrin and a metal ion produces a metalloporphyrin (MP).

When porphyrins are exposed to light, their electronic and spectrophotometric properties change. More specifically, porphyrins absorb certain wavelengths of light and reflect others, which give porphyrins their characteristic colors visible to the human eye. The spectrophotometric properties allow porphyrins to absorb both visible and ultraviolet light when illuminated. The ability to absorb light is measured in a technique called absorption spectroscopy. Modulating the optical properties can affect the efficacy of practical applications or ability to bind to other molecules.

Because of the ability to transfer energy from light to oxygen molecules in the surrounding environment, porphyrins find applications in energy transfer processes.[8] When illuminated, porphyrins can acquire energy from light and transfer the energy to an oxygen molecule (Fig. 3).[1] When oxygenated media containing porphyrins are illuminated, the porphyrins jump to an excited electronic state. When the porphyrin returns to the ground state, energy is emitted and transferred to triplet molecular oxygen to produce its excited form: singlet oxygen.[1] This is a high-energy chemical species capable of oxidizing organic molecules in the surrounding environment. This process finds applications in tumor treatment and antibacterial agents.[1-9] This is the basis of Photodynamic Therapy (PDT). Photodynamic therapy provides an alternative way to detect lesions, treat tumors, and treat infectious diseases, with recent studies focusing more on tumor treatment. This new method has fewer side effects and can be used on areas of the body that are difficult to reach with traditional chemotherapy or surgery.[12]

The main components of PDT include the photosynthetizer, light, and oxygen. In this case, the porphyrin is the photosynthetizer. The singlet oxygen is believed to be toxic to tumor cells because it causes vascular shutdown and modulates the apoptotic and necrotic cell mechanisms.[1,12] Moreover, the addition of a metal catalyzed this process.[4] This could lead to an increase in singlet oxygen yields, ultimately leading to more effective treatment. Thus, it is generally important to be able to modulate porphyrin optical properties by adding other molecules or changing environmental conditions for practical applications.[2, 4,5, 8, 10-11]

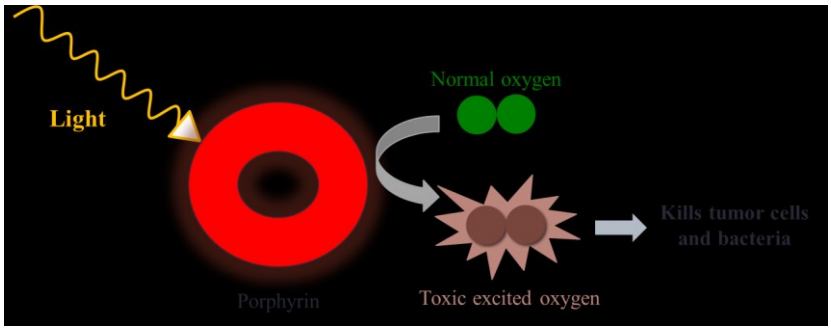

Figure 3 – Light is absorbed by a porphyrin. The acquired energy is transferred to a normal oxygen molecule leading to the formation of a toxic excited oxygen molecule.

For these studies, it is important to investigate the physical chemical behavior of porphyrins in aqueous solutions. Because it is important to study aqueous solutions for biological relevance, porphyrins must be soluble in water. Solubility is increased by functionalizing porphyrins with ionic chemical groups. This will lead to porphyrins having polar and nonpolar regions. Nonetheless, the amphiphilic nature of this organic molecule will still lead to self-aggregation in water. Ultimately, this self-aggregation will lead to the formation of water-soluble large aggregates of porphyrins. The aggregation of these porphyrins is driven by π-π interactions. This π-π stacking is due to the attractive,

noncovalent interactions between the delocalized π orbitals of the aromatic rings. The efficacy and association of these porphyrins depends on porphyrin environment. When porphyrins stack on each other, the shape of aggregates is affected by the electrostatic interactions between the charged functional groups of the molecule, which are located on the periphery, and the positively charged core (Fig. 4). These aggregates cause known shifts in the spectrophotometric properties. For example, the presence of blue shifts or red shifts has been correlated to hypsochromic (H-) and bathochromic (J-) aggregates, respectively.[13]

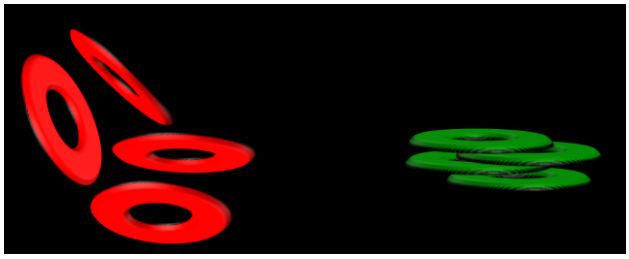

Figure 4 – Individual porphyrin molecules associate in water to form aggregates.

As previously mentioned, it is important to investigate additives (e.g. salts, polymers, detergents, micelles) that can modulate porphyrin self-aggregation. Previous studies have aimed at modulating porphyrin self-aggregation by the addition of molecules in solution such as surfactants or polymers.[4,10] Self-aggregation can also be affected by pH, metal ions, concentration, temperature, and ionic strength.[13] This project quantitatively examines how polymers can be used to reduce porphyrin self-aggregation. Understanding the connection between porphyrin self-aggregation and polymer-porphyrin binding will ultimately provide knowledge for applications such as PDT. Furthermore, our thermodynamic analysis will allow us to determine the relative contribution of enthalpic versus entropic effects in these interactions.

One of the major factors influencing aggregation is the pH of the solution. The primary method of determining the effects of the acidity or basicity of the environment on the porphyrin is by comparing the porphyrin pK_a to the pH. The pK_a is a quantitative measurement of acidity. Thus, environment influences porphyrin electrostatic interactions because porphyrins can exist in a deprotonated and a protonated state. At a high or low pH relative to the pK_a, the porphyrin molecule can have a larger charge difference between the core and the surrounding part of the molecule. These electrostatic interactions can affect porphyrin aggregation.

This study focuses on meso-tetrakis(4-sulfonatophrnyl)porphyrin (TPPS) (Fig. 5) because it is commercially available and water-soluble. This water solubility is not common among porphyrins and can be attributed to the four negatively charged sulfonic groups on the periphery. The main factor influencing aggregation is the protonation state of the four pyrrole nitrogens in the TPPS core. When all of the nitrogens are protonated at low pH, the overall molecule has a -2 net charge. However, when only two nitrogens are protonated at high pH, the overall molecule has a -4 net charge. Hence, the electrostatic repulsion between two molecules is lower at low pH. The decrease in electrostatic repulsion enhances self-association through π-π orbital stacking.[2,5,16]

There are two pK_a values that can be associated with this TPPS core. Since both pK_a's have a value of about 5,[10,13,17] the change in the net charge occurs around pH ≈ 5 (Fig. 5).

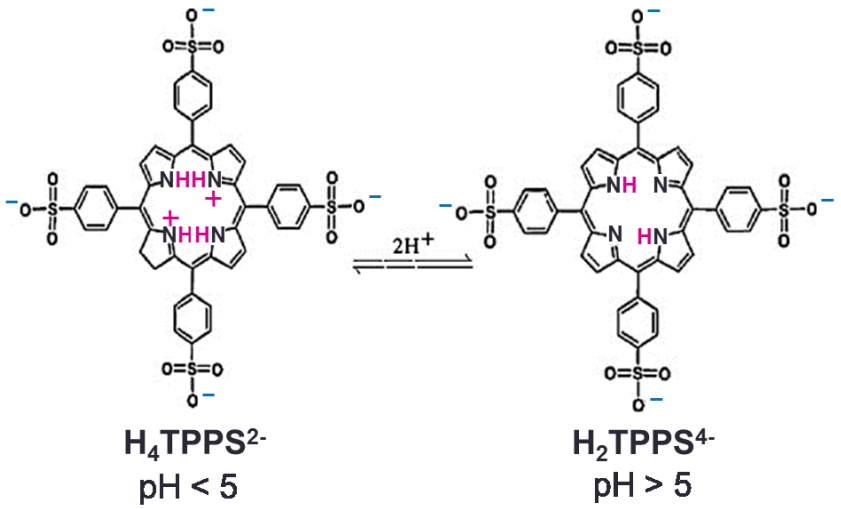

Figure 5 – The molecule used in this study, TPPS, is shown in the tetraprotonated state at pH < 5 and the diprotonated state at pH > 5. The overall charge of the molecule is -2 and -4 in the tetraprotonated and diprotonated state, respectively. The electrostatic repulsion between TPPS molecules is lower when in the tetraprotonated state.

Aggregation states of TPPS, the presence of cationic species, the ability to generate singlet oxygen for PDT, and other environmental factors such as organic solvent and temperature have been investigated in previous TPPS studies.[5,7,9,10,13,17] However, little work has been performed on the effects of polymers on porphyrin aggregation behavior. This project attempts to clarify how polymers will affect porphyrin aggregations based on absorption spectroscopy and isothermal titration calorimetry.

Absorption spectroscopy has been used to characterize the aggregation states. The wavelengths of interest include the Q bands at 500-700 nm and the Soret band at 400-450 nm. The presence and shifts of these bands provide information that helps determine porphyrin aggregation state. Specifically, the Q bands include the Q_X and Q_Y bands. The Q_X bands correspond to electronic transitions along the x-axis. This is parallel to the permanently protonated pyrrole nitrogens by convention.[15] The Q_Y bands correspond to transitions parallel to the other two nitrogen atoms (Fig. 6).

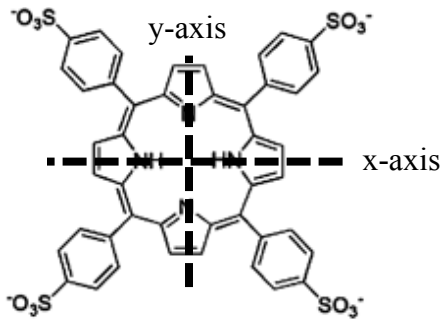

Figure 6 – The axes of TPPS are shown. The permanently protonated nitrogens are located on the x-axis.

Shifts in the Q band region will show that the associated hydrogens affect the aggregation state. If one porphyrin molecule binds to another molecule along the x-axis or y-axis, then the corresponding Q_X or Q_Y bands will show an appreciable shift. The Soret band has the same function and will change similarly to the Q bands. In Fig. 7, the energy diagram describing the electronic transitions corresponding to the Q and Soret bands is shown. The vertical arrows in the figure describe the transitions corresponding to the absorption of photons with wavelength λ. The observed wavelength in the absorption spectrum is given by $\Delta E = hc/\lambda$ (Bohr condition), where ΔE is the difference in energy between excited and ground states, h is Planck's constant, and c is the speed of light.

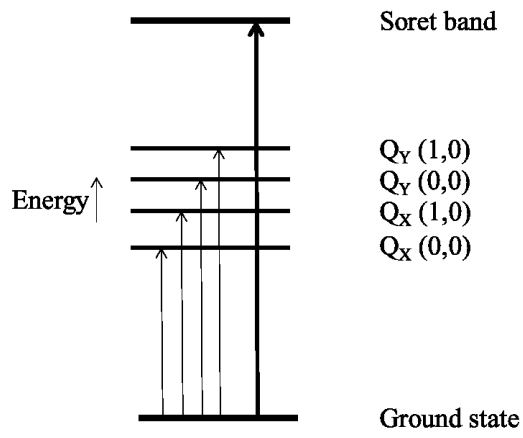

Figure 7 – The energy diagrams of Q_X and Q_Y, and Soret regions corresponding to specific regions on the absorption spectra. The wavelength can be related to the energy of a photon and the speed of light. Thus, the higher energy differences correspond to lower wavelengths. The energy jumps from ground state to Q_X and Q_Y (0,0) include the jump from the ground electronic, ground vibrational state to the excited electronic, ground vibrational state. The energy jumps from ground state to Q_X and Q_Y (1,0) include the jump from the ground electronic, ground vibrational state to the excited electronic, excited vibrational state.

Thus, absorption spectroscopy provides information on absorbance which can provide information on the energy of the solution through the Beer-Lambert Law (Abs = $\varepsilon(\lambda)\, l c$), where Abs is the sample absorbance measured using a spectrophotometer, $\varepsilon(\lambda)$ is the wavelength-dependent extinction coefficient, l is the length that the photons travel inside the investigated sample, and c is the known concentration of the investigated solute (TPPS).

Polymers have a plethora of practical applications such as pharmaceuticals, food, textiles, medicine, and plastics.[10,19] The polymer of interest is polyvinylpyrrolidone (PVP), which is one of the most common biocompatible hydrophilic neutral polymers. It also serves as a solubilizing agent, which can improve dissolution of porphyrins in aqueous solution. PVP has shown to have practical applications, the most important being biocompatibility and mechanical properties in tablet formations.[19] The PVP monomer chemical structure

has a 5 membered ring with an amide nitrogen connecting to the carbon backbone (Fig. 8). The polymeric structure of PVP structure in water resembles that of a coil (Fig. 9).

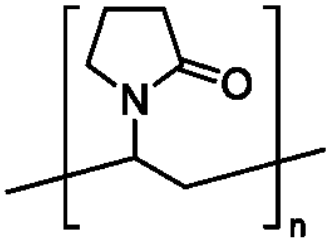

Figure 8 – The monomeric chemical structure of PVP, where *n* represents the number of monomers in a polymer chain.

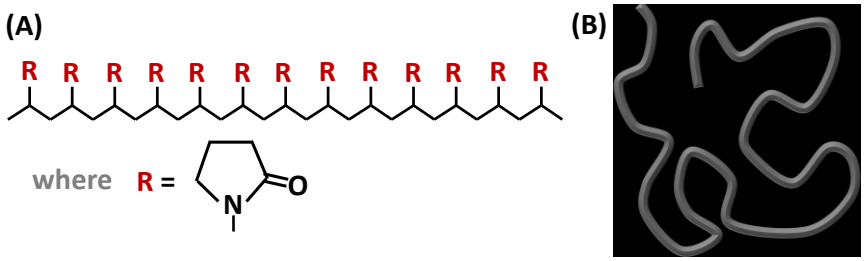

Figure 9 – **A)** Chemical structure of the chosen polymers (PVP) for these studies. **B)** PVP can be approximately described as a flexible coil in water. In this work, number of monomers that constitute a polymer is 160 (MW: 40 kg mol^{-1}).

This coil interaction with the porphyrin should affect aggregation.[2] Additionally, the PVP molecule absorbs very little light so it should not interfere with the absorption spectrophotometric properties of the porphyrin. Our study examines the capabilities of PVP in modulating the TPPS aggregation state.

Furthermore, we have used ITC to investigate the effect of PVP on TPPS absorption-spectroscopy properties at pH 7.0. The results from this technique allow us to determine the strength of binding.[20,21] Specifically, this technique will allow us to determine the equilibrium constant (K), number of binding sites on the polymer (n), and

the heat of reaction ($\Delta_r H°$). The understanding of these properties will elucidate the relative strength of porphyrin self-association and porphyrin-polymer binding.

A given ITC experiment allows us to determine n, K, and $\Delta_r H°$ at one temperature. Experiments at different temperatures provide information on the temperature dependence of these parameters. It is important to remark that the temperature dependence of K can also be used to extract $\Delta_r H°$ (Van't Hoff law). Thus, ITC provides two *independent* ways to extract heats of reaction. This is valuable because the comparison between the two obtained values of $\Delta_r H°$ can be used as a criterion to assess the accuracy of the model used to describe the complex chemical equilibrium occurring in these polymer-porphyrin aqueous mixtures. ITC also gives very precise values of $\Delta_r H°$. This is important to characterize reaction entropy, $\Delta_r S°$, and reaction heat capacity $\Delta_r C_p$. This is valuable for the evaluation of hydrophobic interactions in porphyrin-porphyrin and polymer-porphyrin interactions in aqueous solutions.

Other studies have investigated porphyrin-polymer interactions,[2,10,14] but this is the first to use both absorption spectroscopy and ITC to characterize porphyrin aggregation and polymer-porphyrin binding.

EXPERIMENTAL SECTION

Materials

Tetrasodium tetraphenylporphyrin tetrasulfonate or 5,10,15,20-Tetraphenyl-21H, 23H-porphine-p-p',p'',p'''-tetrasulfonic acid tetrasodium hydrate (molecular weight = 1023 kg mol^{-1}) (>0.99 mass fraction purity) (specific volume = 0.78 cm^3 g^{-1}) was purchased and used without further purification from Sigma-Aldrich (Missouri, USA). TPPS was mixed with deionized water to form a ~1% stock solution by weight.

Subsequent stock solutions of ~0.1%, ~0.05%, and ~0.025% TPPS were prepared by dilution of the 1% solution. Polyvinylpyrrolidone (molecular weight = 111.14 kg mol^{-1}) (specific volume = 0.999 cm^3 g^{-1}) was also obtained from Sigma-Aldrich and used without further purification (>0.99 mass fraction purity). PVP was mixed with deionized water to form a ~10% stock solution by weight. Subsequent stock solutions of ~2%, ~1%, ~0.1%, and ~0.02% PVP were prepared by dilution of the stock solution. Buffers of pH 3.0, 4.5, and 7.0 were prepared used in order to maintain a constant pH in the solutions. The solutions examined in ITC and absorption spectroscopy involved mixing known amounts of TPPS, PVP, buffer, and water by weight. At pH 7.0, a 0.10 M sodium phosphate buffer was used to make the phosphate concentration 0.010M in the solution. At pH 4.5, sodium acetate buffer was used to make the acetate concentration 0.010M in the solution. At pH 3.0, citric acid buffer was used to make citrate concentration 0.010M in the solution. The water used was deionized and purified through a four-stage Millipore filter system to ensure high water purity. TPPS-PVP solutions were also prepared by weight.

Methods

Preparation of TPPS-PVP solutions

The TPPS-PVP solutions were prepared mixing the stock solutions. The PVP molar concentration was varied from 0% to 0.08% by weight while the TPPS concentration was kept constant in three series of solutions at 0.025%, 0.05%, and 0.1% by weight. Samples were prepared at pH values of 3.0, 4.5, and 7.0. The pH values of the TPPS-PVP were addressed by adding a phosphate buffer solution (0.100 M, pH 7.0), acetate buffer solution (0.100 M, pH 4.5), or citric acid buffer solution (0.100 M, pH 3.0).

The final buffer concentration of all TPPS-PVP solutions was 0.010M. The pipettes used included 20, 100, 200, and 1000μl pipettes to gravimetrically mix known amounts of TPPS stock solutions, PVP stock solutions, buffer, and water together. Absorption spectroscopy measurements of these solutions were taken within two hours of preparing these solutions.

Measurements of Absorption Spectroscopy

The absorption spectroscopic measurements were made on a UV-Vis DU800 Spectrophotometer (Beckman-Coulter) using cuvettes with 1 cm and 1 mm of path length, at 22.5 °C. The wavelengths of interests included Q bands at 500-700 nm and the Soret band at 400-450 nm and cuvettes with path lengths of 1 cm and 1 mm were used to take spectroscopic measurements, respectively. After absorption curves were obtained, the results were normalized and the molar absorption coefficient (ε) was calculated with: $\varepsilon = Abs/(lC)$, where *Abs* is absorbance of the sample, C is TPPS concentration of the sample, and *l* is the path length of the cuvette used in the spectrophotometer.

Measurements of ITC

An isothermal titration calorimeter MicroCal ITC_{200} (Microcal Inc., Northampton, MA) from GE Healthcare Life Sciences was used. TPPS dissociation and TPPS-PVP binding experiments were performed at 12, 25, and 37 °C and atmospheric pressure (~0.99 bar).

In this isothermal technique, the sample cell and the reference cell are kept at the same temperature. The titrant is aliquotted into the titrand and the reaction between the titrant and titrand is either endothermic or exothermic. If the reaction is endothermic, the sample cell needs more energy to remain at the same temperature as the reference cell. If

the reaction is exothermic, the cell will need less energy to remain at the reference cell temperature.

In the dissociation experiments, TPPS aliquots (2.0 μL, 3.69 mM) were sequentially injected (~20 injections) from a rotating syringe into a stirred sample (syringe rotation = 1000 rpm) of 0.010-M buffer solution. TPPS dilution leads to disaggregation, resulting in the isothermal absorption of heat from surroundings.

In the TPPS-PVP binding experiments, PVP was chosen as the titrant and TPPS was chosen as the titrand. The titrant is sequentially aliquotted into the titrand. PVP was chosen as the titrant because after preliminary experiments, PVP dilution causes a negligible contribution to overall reaction heat. On the other hand, TPPS dilution would cause TPPS endothermic dissociation that would contribute to the reaction cell heat. The small dilution of TPPS made the measured heat of reaction higher than the reaction between TPPS and PVP. The heat of PVP dilution to PVP-TPPS binding was small compared to TPPS dilution. The dilution enthalpies determined in this control experiment were subtracted from the enthalpies of the PVP-TPPS titration experiments.

Each microcalorimetric titration experiment consisted of roughly twenty successive injections of 2.0 μL of PVP solutions into the reaction cell containing a known amount of TPPS. A rotating syringe stirred the sample cell (syringe rotation = 1000 rpm). The reaction cell (203.4 μL by factory specifications) was loaded with a known concentration of TPPS solution. All buffer solutions had the same concentration. The equilibrium constant (K), the binding stoichiometry (n), and the molar enthalpy ($\Delta_r H°$) were obtained from the titration curve using the ORIGIN software supplied by Microcal Inc. Further data analysis was performed using MATLAB.

On the injection plots, the peaks represent injections. Each injection shows work as a function of time. The integral of this gives the power needed to keep the reference and sample cells at the same temperature. The differential heat is calculated as the area of the corresponding peak. This is normalized with respect to moles of titrant. The differential heat $q^{(i)}$, with injection i, correlates to cumulative heat $Q^{(i)}$ of the sample cell by:

$$q^{(i)} = [(V + v/2)(Q^{(i)}/V) - (V - v/2)(Q^{(i-1)}/V)]/(v\,C'_{\mathrm{TITRANT}}) \qquad (1)$$

where $Q^{(0)} = 0$, V represents the volume of the sample cell (203.4 μM), v represents the volume of individual titrant injections, and $C'_{TITRANT}$ is concentration of titrant. $(V + v / 2)$ and $(V - v / 2)$ represent the corrections taken into account when the titrant displaces the titrand in the sample cell, displacing a small fraction (v / V ≈ 0.01) to the outside of the sample cell into the neck of the reaction container. Thus, when injection i occurs, some of the reaction heat taken into account comes from injection $(i - 1)$ because the displaced sample in $(i - 1)$ will contribute to injection i reaction heat. This overestimates the actual reaction heat or $Q^{(i)}$. In $(i - 1)$, some of the reaction is displaced into the neck and does not contribute to $Q^{(i-1)}$. Thus, $Q^{(i-1)}$ is underestimated. The two components of $(V \pm v/2)/V$ in (*1*) represent the average between the mixing before and after sample displacement.

Binding models are used to obtain expressions that link $Q^{(i)}/V$ to $C^{(i)}_{TITRANT}$ (titrant) and $C^{(i)}_{TITRAND}$ (titrand) inside the sample cell after injection i. These can be calculated by using:

$$C^{(i)}_{\text{TITRANT}} = [i\,v/(V + i\,v/2)]\; C'_{\text{TITRANT}} \tag{2}$$

$$C^{(i)}_{\text{TITRAND}} = [(V - i\,v/2)/(V + i\,v/2)]\; C'_{\text{TITRAND}} \tag{3}$$

where $C'_{TITRAND} = C^{(0)}_{TITRAND}$ is the initial concentration of titrand within the sample cell. Equations 2 and 3 are the averages between two limiting mass balances. Equation 2 regards the titrant and is the average between mixing before sample displacement [$(V + i\,v)\,C^{(i)}_{\text{TITRANT}} = i\,v\;C'_{\text{TITRANT}}$] and the mixing after sample displacement [$V\,C^{(i)}_{\text{TITRANT}} = i\,v\;C'_{\text{TITRANT}}$]. Equation 3 regards the titrand and is the average between mixing before sample displacement [$(V + i\,v)\,C^{(i)}_{\text{TITRAND}} = V\;C'_{\text{TITRAND}}$] and the mixing after sample displacement [$V\,C^{(i)}_{\text{TITRAND}} = (V - i\,v)\;C'_{\text{TITRAND}}$].

RESULTS

Absorption Spectroscopy

Normalized absorption spectra in the visible wavelength range are shown for increasing concentration of TPPS in aqueous solution (Fig. 10) and PVP-TPPS aqueous solutions (Fig. 11). All absorption spectra for PVP-TPPS interactions are reported in Appendix A. The effect of pH on the absorption properties of TPPS in the absence and presence of PVP are shown in Fig. 12. Then, the shifts in the Q and Soret band region are examined in the discussion (Figs. 15 & 16). These experiments were performed at room temperature (22.5±0.5 °C).

In Fig. 10, it is interesting to note that as TPPS concentration increases, the spectrum shifts toward higher wavelengths.

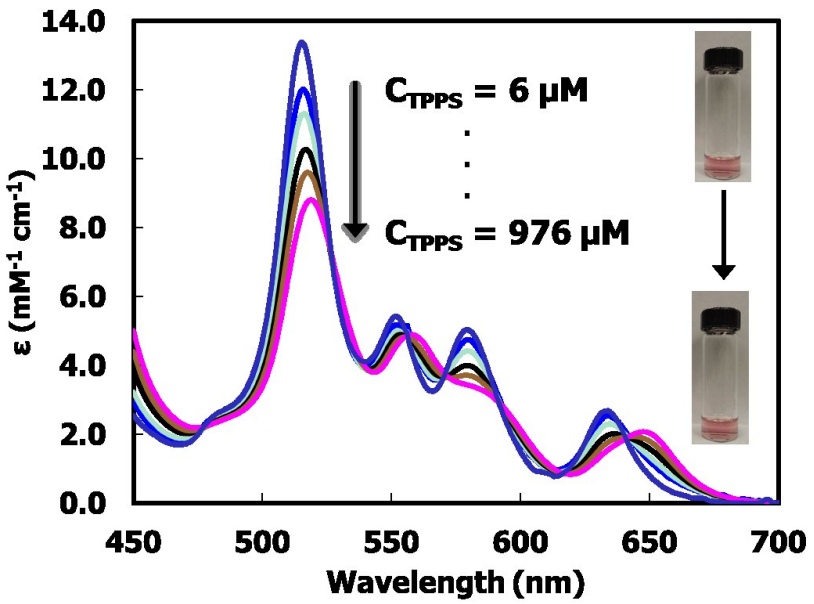

Figure 10 – Normalized absorption spectra are shown with extinction coefficient ε as a function of wavelength. Initial concentration of TPPS (C_{TPPS}) started at 6 μM and was increased to 976 μM at pH 7.0. Pictures of the low concentration and high concentration prepared solutions are shown, with the uppermost vial representing the low concentration and the lower vial representing the high concentration. The presence of isosbestic points shows that there are only two species in solution: TPPS monomer and aggregate.

In the absence of TPPS aggregation, all spectra are expected to overlap. Thus, the observed shifts can be attributed to TPPS self-association.

In Fig. 11, it is interesting to note that as PVP concentration increases, the spectrum shifts toward a higher wavelength. The spectral shifts show that there is an interaction between the TPPS molecules and PVP. This interaction can be attributed to TPPS-PVP association that competes with TPPS self-association.

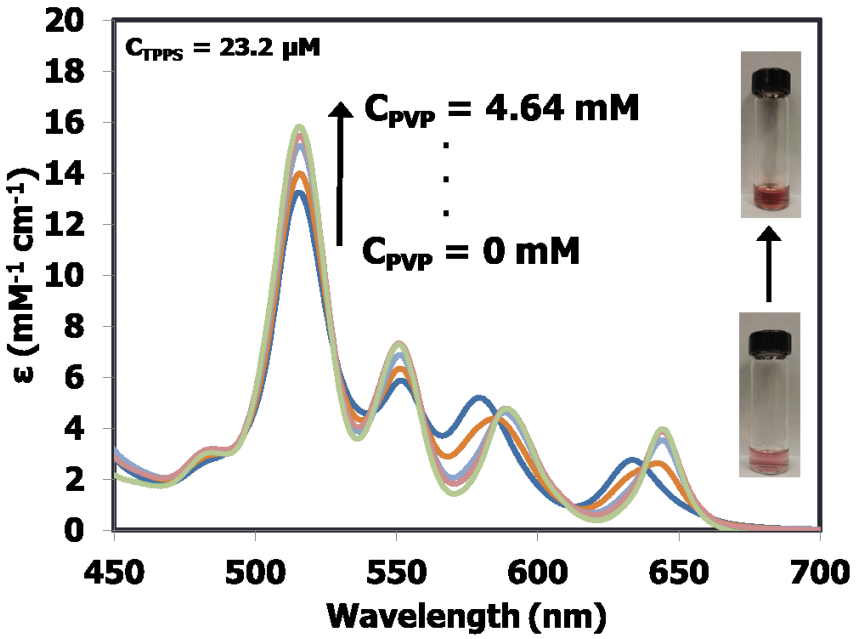

Figure 11 – Normalized absorption spectra are shown with extinction coefficient ε as a function of wavelength. Concentration of TPPS (C_L) was held constant at 23.2 mM at pH 7.0. PVP concentration was increased from 0 mM to 4.64 mM. Pictures of the low concentration and high concentration prepared solutions are shown, with the lower vial representing the low concentration and the upper vial representing the high concentration.

The pH of solution can have effects on the TPPS spectra. The TPPS molecule has two values similar to each other around 5, so the protonation of the molecule will affect TPPS self-association. In Fig. 12, absorbance at higher wavelengths is enhanced as pH decreases. However, as PVP concentration increased, the effects of pH were diminished. The resulting spectra overlapped, regardless of pH at $C_{PVP} = 4.64$. Qualitatively, the TPPS-only solutions had different colors, with the more acidic solutions having a green color and the solution at pH 7.0 having a light red color. As PVP concentration increased, the three solutions appeared to have the same dark red color.

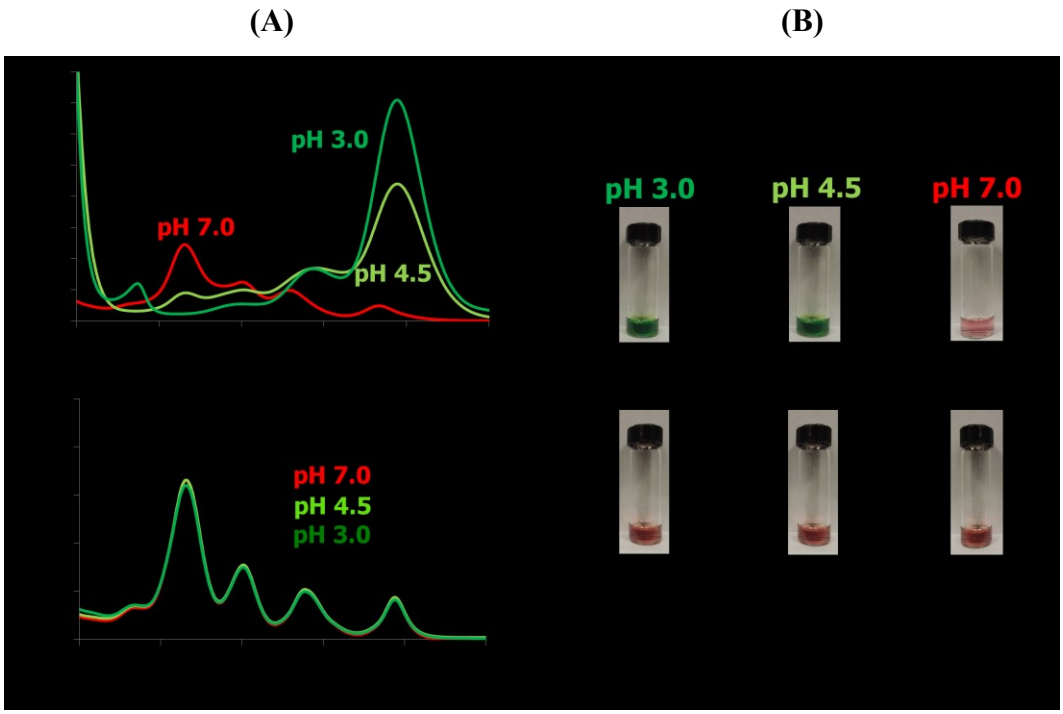

Figure 12 – **(A)** Normalized absorption spectra are shown with extinction coefficient ε as a function of wavelength. Three solutions were prepared at pH 3.0, 4.5, and 7.0. Absorption spectra were taken in order to examine the effects of PVP on pH. In the first graph, TPPS concentration is held constant at 23.2 mM and PVP concentration is zero for all three solutions. In the second graph, C_{TPPS} = 23.2 mM and C_{PVP} = 4.64 mM for all three solutions. Concentration of TPPS (C_L) was held constant at 23.2 mM at pH 7.0. PVP concentration was increased from 0 mM to 4.64 mM. **(B)** Pictures of the low concentration and high concentration prepared solutions are shown. As the PVP concentration of solution increased, the colors of the vials appeared more similar. This was represented graphically in the second graph of Fig. 12A.

Isothermal Titration Calorimetry

Figure 13 shows the ITC experiments and the corresponding Van't Hoff plot for TPPS dissociation experiments. In Fig. 13A, differential heat plots are shown for ITC dissociation experiments of TPPS at 12, 25, and 37 ºC. The positive values show that TPPS dissociation is an endothermic process. At higher temperatures, more heat is absorbed upon dissociation. In Fig. 13B, $R\ln(\alpha_{dim})$ is plotted as a function of 1/T, where R represents the ideal-gas constant and *T* represents temperature. This second plot will be explained and examined in the discussion section.

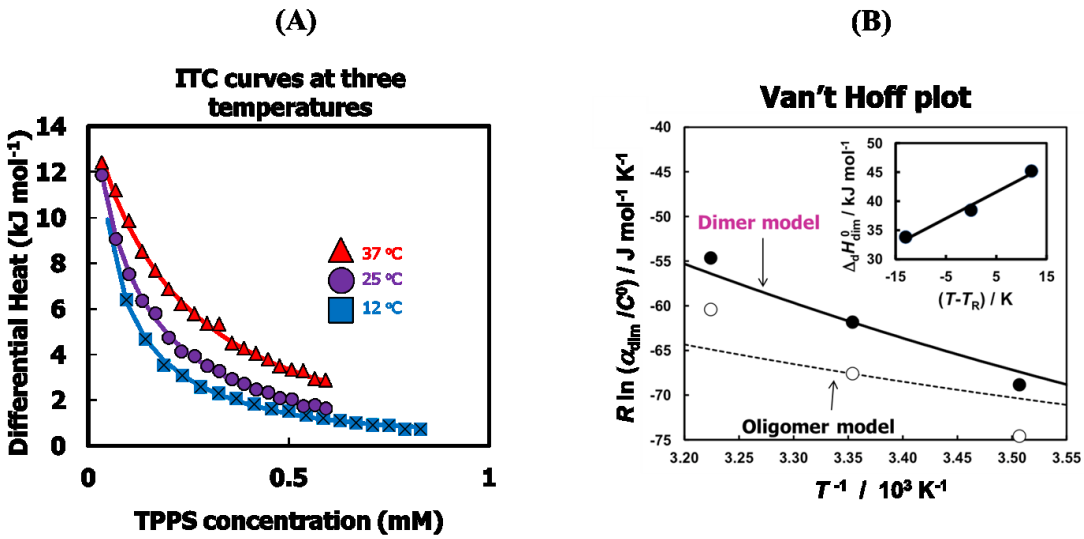

Figure 13 – **(A)** Differential heat is determined from consecutive aliquots of titrant (TPPS, 3.69 mM; sodium phosphate buffer, 10 mM, pH 7.0) into titrand (sodium phosphate buffer, 10 mM, pH 7.0) as a function of TPPS concentration. The different temperatures are shown at 12 °C (blue squares), 25 °C (purple circles), and 37 °C (red triangles). As more TPPS is aliquotted into the titrand, the differential heat decreases, showing that the dissociation is not as strong. **(B)** The Van't Hoff plot for the TPPS dimer dissociation constant is shown as a function of temperature. The solid line shows the predicted behavior of α_{dim} at 25 °C from the corresponding reaction enthalpy and heat capacity values obtained from the ITC experiments. The solid circles show the results from ITC experiments. Consequently, the oligomer or equal-constant self-association model is shown. The experimentally determined values are shown with the open circles and the predicted α_{olig} behavior is shown in the dashed line. Standard concentration was kept at C° ≡ 1M and reference temperature was T_R ≡ 25 °C. The inset shows standard dissociation enthalpy as a function of temperature. The increasing slope shows that heat capacity increases as temperature increases.

Figure 14 shows the ITC experiments and corresponding Van't Hoff plot for TPPS dissociation experiments. In Fig. 14A, differential heat plots are shown for ITC experiments of PVP aliquots into TPPS at 12, 25, and 37 ºC. The negative values show that TPPS-PVP interactions are exothermic processes. At higher temperatures, more heat is released upon TPPS-PVP binding interaction. In Fig. 14B, Rln(K) is plotted as a function of 1/T. This second plot will be explained and examined in the discussion section.

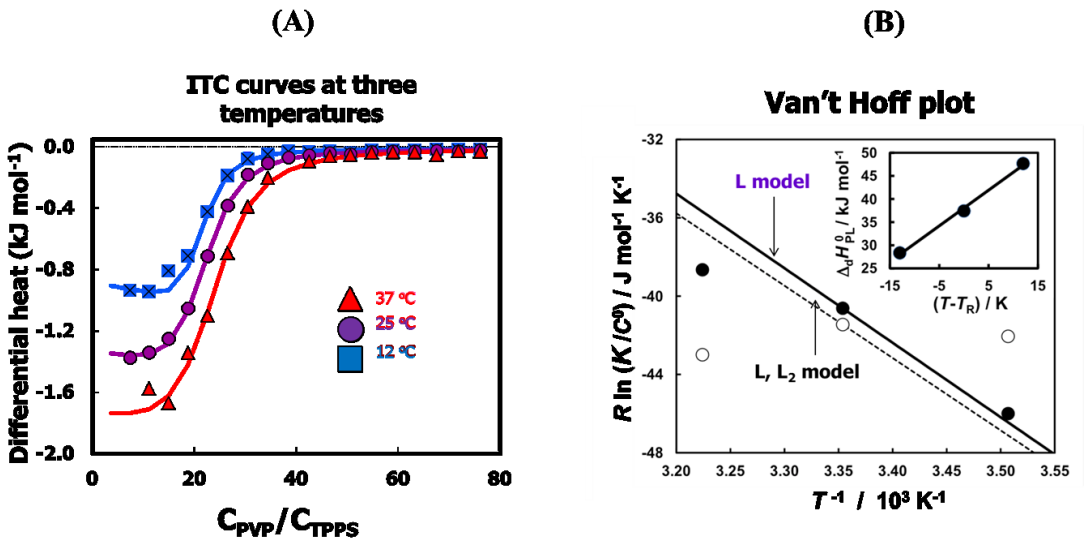

Figure 14. **(A)** Differential heat is determined from consecutive aliquots of titrant (PVP, 91.0 mM; sodium phosphate buffer, 10 mM, pH 7.0) into titrand (TPPS, 0.244 mM; sodium phosphate buffer, 10 mM, pH 7.0) as a function of the ratio of PVP to TPPS concentration after injection. These experiments were performed at three different temperatures, shown at 12 °C (blue squares), 25 °C (purple circles), and 37 °C (red triangles). As more PVP is aliquotted into the titrand, the differential heat decreases, showing that the PVP-TPPS binding is not as strong. **(B)** The Van't Hoff plot for the PVP-TPPS dissociation constant, K, is shown as a function of temperature. The L model says that only TPPS monomers bind to PVP. The solid line represents the L model and shows the predicted behavior of K at 25 °C from the corresponding reaction enthalpy and heat capacity values obtained from the ITC experiments. The solid circles show the results from ITC experiments. Consequently, the L, L_2 model that says TPPS monomers and dimers bind equally to PVP is shown. The experimentally determined values are shown with the open circles and the predicted K behavior is shown in the dashed line. Standard concentration was kept at C° ≡ 1M and reference temperature was T_R ≡ 25 °C. The inset shows standard dissociation enthalpy as a function of temperature. The increasing slope shows that heat capacity increases as temperature increases.

Table 1. Thermodynamic parameters associated with TPPS dimerization.

T / K	285.15	298.15	310.15
α_{dim} / mM	0.25±0.01	0.58±0.02	1.4±0.1
$\Delta_{\mathrm{d}}H^{0}_{\mathrm{dim}}$ / kJ mol^{-1}	33.9±0.4	38.5±0.4	45.2±0.4
$\Delta_{\mathrm{d}}G^{0}_{\mathrm{dim}}$ / kJ mol^{-1}	19.6±0.08	18.5±0.08	16.9±0.17
$\Delta_{\mathrm{d}}S^{0}_{\mathrm{dim}}$ / J mol^{-1} K^{-1}	50±1	67±1	91±1
α_{dim} / mM (calc)	0.300	-	1.13

Table 2. Thermodynamic parameters associated with PVP-TPPS binding.

T / K	285.15	298.15	310.15
$1/n$	18.7±0.2	19.6±0.2	21.8±0.4
K / μM	3.9±0.5	7.5±0.5	9.5±1.5
$\Delta_{\mathrm{d}}H^{0}_{\mathrm{PL}}$ / kJ mol^{-1}	28.5±0.3	37.4±0.3	47.7±1.0
$\Delta_{\mathrm{d}}G^{0}_{\mathrm{PL}}$ / kJ mol^{-1}	29.5±0.3	29.3±0.2	29.8±0.4
$\Delta_{\mathrm{d}}S^{0}_{\mathrm{PL}}$ / J mol^{-1} K^{-1}	-4±2	27±1	58±4
K / μM (calc)	3.73	-	13.6

DISCUSSION

TPPS self-association

In Fig. 10, the increase in TPPS concentration resulted in spectral shifts. This can be attributed to TPPS self-association. Previous studies have shown that TPPS aggregates through edge-to-edge stacking.[9] To minimize electrostatic repulsion, two porphyrin molecules will stack by the sulfonate group of one porphyrin interacting with the positively-charged core of the other porphyrin. Due to steric considerations, TPPS can associate in dimers or higher-order oligomers. ITC plots and the Van't Hoff law allowed for the determination of the more accurate binding models regarding TPPS self-association: the dimerization model[21] or the equal-constant self-association (oligomer) model[22]. In Fig. 13, the differential heat plots were examined to evaluate both models.

In the dimerization model: $L_2 \leftrightarrows 2L$, where L and L_2 represent the TPPS monomer and dimer, respectively. The cumulative heat for dissociation of TPPS dimers is represented by:

$$\frac{Q}{V} = ([L_2] - [L_2]_0)\Delta_d H^0_{dim} \quad (4)$$

where $[L_2]$ represents dimer concentration in the reaction cell, $[L_2]_0$ is the hypothetical concentration of dimers in the sample cell calculated by assuming that all dimers transferred from the titrant solution do not dissociate, and $\Delta_d H°_{dim}$ represents the standard enthalpy of dimer dissociation. Because there is one bonding interaction in every molecule, Q/V is directly related to dimer concentration. The mass action law allows us to introduce the dimer dissociation constant, α_{dim}, and link the monomer concentration, [L], to that of the dimer, $[L_2]$, given by:

$$\alpha_{dim} = \frac{[L]^2}{[L_2]} \quad (5)$$

Monomer concentration relates to known total concentration of TPPS (C_L) by the mass balance:

$$\frac{\alpha_{dim}}{[L]} = 1 + 2\frac{[L]}{\alpha_{dim}} \quad (6)$$

which can be rearranged to solve for [L].

$$[L] = \frac{\alpha_{dim}}{4}\left(\sqrt{1 + \frac{8C_L}{\alpha_{dim}}} - 1\right) \quad (7)$$

In eq. 4, $[L_2]_0$ is determined by calculating the dimer concentration in the titrant solution and then applying the dilution factor in eq. 2. Equations 5 and 7 are used in order to determine $[L_2]$ in eq. 4.

In Table 1, the experimentally determined values of α_{dim} and $\Delta_d H°_{dim}$ are shown. As temperature increases, α_{dim} increases. In other words, as temperature increases, the concentration of monomer to dimer increases, consistent with TPPS dissociation being endothermic. After determining the dimerization constant and enthalpy of dimerization, standard Gibbs free energy and entropy values were calculated by using $\Delta_d G^0_{dim} = -RT \ln \alpha_{dim}$ and $\Delta_d S^0_{dim} = (\Delta_d H^0_{dim} - \Delta_d G^0_{dim}) / T$ where R is the ideal-gas constant and T is the absolute temperature. Then, constant-pressure heat capacity of dissociation, $\Delta_d C^0_{p,dim} = (0.45 \pm 0.06)\,\mathrm{kJ\,mol^{-1}K^{-1}}$, was determined by using $\Delta_d H^0_{dim} = \Delta_d H^0_{dim,R} + \Delta_d C^0_{p,dim} \cdot (T - T_R)$ where T_R = 298.15 K and $\Delta_d H^0_{dim,R} = (39.3 \pm 0.6)\,\mathrm{kJ\,mol^{-1}}$ was the value at T_R extracted from the fit.

The theoretical behavior of the dimerization model from the determined values of $\Delta_d S^0_{dim,R}$, $\Delta_d H^0_{dim,R}$, and $\Delta_d C^0_{p,dim}$ are related to the dissociation constant by the Van't Hoff law:

$$R \ln \alpha_{dim} = \Delta_d S^0_{dim,R} - \frac{\Delta_d H^0_{dim,R}}{T} - \Delta_d C^0_{p,dim} \cdot \left(\frac{T - T_R}{T} - \ln \frac{T}{T_R} \right) \tag{8}$$

where $\Delta_d S^0_{dim,R}$ (70±3) J mol^{-1} K^{-1} at T_R = 298.15 K from values in Table 1 and $\Delta_d C^0_{p,dim}$ is assumed to be independent of temperature. In Fig. 13B, this theoretical curve is plotted with experimental values of $R \ln \alpha_{dim}$. The error of experimental values to theoretical values is lower than 20%, which we believe to be an acceptable difference for experimentally determined equilibrium constants.

In the equal-constant self-association model: $L_k = L_{k-1} + L$ (k = 2, 3, 4,…), where L represents TPPS, neglecting the formation of cyclic assemblies. Consequently, the oligomer dissociation constant, α_{olig}, can be represented by:

$$\alpha_{\text{olig}} = \frac{[\text{L}][\text{L}_{k-1}]}{[\text{L}_k]} \qquad \text{where } k = 2, 3, 4, ... \tag{9}$$

The cumulative heat for the dissociation of TPPS oligomers can be represented by:

$$Q/V = \left(\sum_{k=2} (k-1)[\text{L}_k] - \sum_{k=2} (k-1)[\text{L}_k]_0 \right) \Delta_{\text{d}} H^0_{\text{olig}} \tag{10}$$

where $[\text{L}_k]$ is concentration of oligomer k in the sample cell, $[\text{L}_k]_0$ is the hypothetical oligomer concentration in the sample cell assuming all oligomers do not dissociate, and $\Delta_{\text{d}}\text{H}^0_{\text{olig}}$ represents the standard enthalpy of dissociation of a monomer from the oligomer.

The TPPS monomer concentration is related to C_{L} by the mass balance: $C_{\text{L}} = [\text{L}_k] + \Sigma_{k=2} k[\text{L}_k]$. Consequently, $\sum_{k=2} k[L_k]$ can be rewritten as a geometric series, given by:

$$\frac{C_{\text{L}}}{[\text{L}]} = \left(1 - \frac{[\text{L}]}{\alpha_{\text{olig}}} \right)^{-2} \tag{11}$$

Rearranging for [L], the following equation can be obtained:

$$[\text{L}] = \frac{\alpha_{\text{olig}}{}^2}{2C_{\text{L}}} \left(1 + \frac{2C_{\text{L}}}{\alpha_{\text{olig}}} - \sqrt{1 + \frac{4C_{\text{L}}}{\alpha_{\text{olig}}}} \right) \tag{12}$$

Then, eqs. 9 and 12 can be utilized to determine $[\text{L}_k]$ in eq. 10.

The dimerization model and equal-constant self-association model can be compared using the ITC data. By using eqs. 5 and 7 in the dimerization model and using eqs. 9 and 12 for the equal-constant self-association model, the following expressions can be obtained:

$$[\text{L}_2] = \frac{[\text{L}]^2}{\alpha_{\text{dim}}} = \frac{\alpha_{\text{dim}}}{8} \left(1 + \frac{4C_{\text{L}}}{\alpha_{\text{dim}}} - \sqrt{1 + \frac{8C_{\text{L}}}{\alpha_{\text{dim}}}} \right) \tag{13}$$

$$\sum_{k=2}(k-1)[\mathrm{L}_k] = \frac{\alpha_{\mathrm{olig}}[\mathrm{L}]^2}{\left(\alpha_{\mathrm{olig}} - [\mathrm{L}]\right)^2} = \frac{\alpha_{\mathrm{olig}}}{2}\left(1 + \frac{2C_{\mathrm{L}}}{\alpha_{\mathrm{olig}}} - \sqrt{1 + \frac{4C_{\mathrm{L}}}{\alpha_{\mathrm{olig}}}}\right) \tag{14}$$

It is interesting to note that, if $\alpha_{\mathrm{olig}} = \alpha_{\mathrm{dim}}/2$ and $\Delta_{\mathrm{d}}H^0_{\mathrm{olig}} = \Delta_{\mathrm{d}}H^0_{\mathrm{dim}}/2$, then eqs. 13 and 14 are identical. The experimentally determined enthalpy values and Van't Hoff predictions can be compared to each other. A smaller discrepancy equates to a more accurate model. Thus, the comparison allows us to identify the better of the two proposed models.

In Fig. 13B, the theoretical curve and experimental data points are shown for both the dimerization model and equal-constant self-association model. Our study shows that the dimerization model is more accurate. This can be attributed to electrostatic repulsion that hinders the formation of strongly charged oligomers.

The experimentally determined value of $\Delta_{\mathrm{d}}H^0_{\mathrm{dim,R}}$ indicates that dimerization is an enthalpically driven process. Additionally, ITC allows for the elucidation of the relationship between $\Delta_{\mathrm{d}}H^0_{\mathrm{dim,R}}$ and temperature (Fig. 13B inset). Increasing the temperature causes an increase in enthalpy of dimer dissociation, which is consistent with hydrophobic interactions between two porphyrins. It is estimated that one water molecule contributes about 13 J mol^{-1} K^{-1} to the heat capacity through the ice-like cage phenomenon. Because the experimentally-determined constant-pressure heat capacity, $\Delta_{\mathrm{d}}C^0_{p,\mathrm{dim}}$, is 30-times bigger than 13 J mol^{-1} K^{-1}, this indicates significant hydrophobic interactions related to dimer dissociation.

Assuming the solvent can be treated as a continuum, the standard translational entropy of 160 J mol^{-1} K^{-1} can be calculated for dissociative processes using the Sackur-

Tetrode equation.[24] This equation uses the actual mass of TPPS and temperature to obtain the value of $\Delta_r S°$ based on translational motion only. Comparing this value to the experimental $\Delta_d S^0_{dim,R}$, the experimental values in Table 1 are significantly lower than 160 J mol^{-1} K^{-1}. This is consistent with the presence of significant hydrophobic interactions.

TPPS-PVP binding

In Fig. 11, PVP-TPPS interactions were characterized at pH 7.0 and room temperature (22.5±0.5 °C). An increase in PVP concentration in a solution with TPPS resulted in spectral shifts toward the red region. This can be attributed to TPPS-PVP interactions favored over TPPS self-association. In order to determine the binding model of how TPPS binds to PVP, ITC measurements were taken. In Fig. 14, differential-heat plots for ITC TPPS-PVP binding experiments are shown at 12, 25, and 37 °C in order to characterize binding. The values obtained were negative, showing that TPPS-PVP association is exothermic. These experimental values were evaluated using the Scatchard model, which assumes binding sites are equivalent and independent of each other. The Scatchard model is as follows: $PL_k = PL_{k-1} + L$[25], where $k = 1,2,3,\ldots,n$, where P represents PVP, and where n represents the total number of sites on the host polymer. Moreover, this model assumes that only TPPS monomers bind to PVP, which will be discussed later in this section.

The cumulative heat for porphyrin-polymer binding can be represented by:

$$Q/V = \left([L_2]-[L_2]_0\right)\Delta_d H^0_{dim} - \nu C_P \Delta_d H^0_{PL} \quad (15)$$

where $[L_2]_0$ represents the concentration of dimers in the sample cell, assuming the dimers do not dissociate after polymer addition, ν represents the number of porphyrin

molecules that are able to bind to one polymer unit, C_p represents the total polymer concentration, and $\Delta_d H°_{PL}$ represents the standard enthalpy for polymer-porphyrin dissociation. Furthermore, eq. 15 shows that the measured heat of polymer-porphyrin interactions involved TPPS dimer dissociation and polymer-porphyrin binding. Total polymer concentration, C_p, is defined with respect to PVP monomer weight. In the Scatchard model, ν is related to free monomer concentration, [L], by:

$$\nu = \frac{n[\mathrm{L}]}{K + [\mathrm{L}]} \tag{16}$$

where K represents the equilibrium constant for porphyrin-polymer dissociation. If the polymer binding site is able to bind to multiple monomers, then n is a fractional number. In other words, the number of monomers that can bind to a single binding site is $1/n$.

The free monomer concentration, [L], is related to C_L by the mass balance:

$$\frac{C_{\mathrm{L}}}{[\mathrm{L}]} = 1 + 2\frac{[\mathrm{L}]}{\alpha_{\mathrm{dim}}} + \frac{n C_{\mathrm{P}}}{K + [\mathrm{L}]} \tag{17}$$

Equation 17 can be rearranged as a cubic equation with respect to [L] and the three roots can be calculated as functions of α_{dim}, K, and n using MATLAB. Free monomer concentration must be low in order to ensure that the concentrations in the mass balance are positive and that the lowest real positive root is taken for [L].

In Table 2, the values of $\Delta_d H°_{PL}$, K, and n are reported. It is interesting to note that K increases as temperature increases. This is consistent with polymer-porphyrin dissociation being an endothermic process. The values of n show that there are roughly 20 PVP molecules that bind to one TPPS molecule. Taking into account the molecular weight of PVP and TPPS, a saturated PVP-TPPS supramolecular structure is ~50% bigger than that of the polymer chain. It is also interesting to note that $1/n$ increases

slightly as temperature increases. The solvent behavior at different temperatures affects polymeric coiling. According to thermodynamic and viscosity experiments,[26] as the temperature increases, the polymer chains fold in, making the polymer binding sites less accessible to porphyrins. Likewise, more PVP monomers contribute to a particular binding site.

By comparing data from Tables 1 & 2, the strength of TPPS-PVP binding can be compared to TPPS dimerization. The heats of reactions of both polymer-porphyrin binding are similar. However, K values are two orders of magnitude smaller than α_{dim}. This means that polymer-porphyrin binding is stronger than porphyrin dimerization due to entropic effects. Calculated values of Gibbs free energy and entropy using $\Delta_{\mathrm{d}}G^{0}_{\mathrm{PL}} = -RT\ln K$ and $\Delta_{\mathrm{d}}S^{0}_{\mathrm{PL}} = (\Delta_{\mathrm{d}}H^{0}_{\mathrm{PL}} - \Delta_{\mathrm{d}}G^{0}_{\mathrm{PL}})/T$, respectively, are reported in Table 2.

The enthalpy of polymer-porphyrin binding increases with temperature, as seen in Table 2 and the inset of Fig. 14B. By plotting enthalpy as a function of temperature, the constant-pressure heat capacity of dissociation, $\Delta_{\mathrm{d}}C^{0}_{p,\mathrm{PL}} = (0.77 \pm 0.04)\,\mathrm{kJ\,mol^{-1}K^{-1}}$, was determined by using $\Delta_{\mathrm{d}}H^{0}_{\mathrm{PL}} = \Delta_{\mathrm{d}}H^{0}_{\mathrm{PL,R}} + \Delta_{\mathrm{d}}C^{0}_{p,\mathrm{PL}} \cdot (T - T_{\mathrm{R}})$, where $\Delta_{\mathrm{d}}H^{0}_{\mathrm{PL,R}} = (38.1 \pm 0.5)\,\mathrm{kJ\,mol^{-1}}$ is the corresponding $\Delta_{\mathrm{d}}H^{0}_{\mathrm{PL}}$ value extracted from the graph. The results show that constant-pressure heat capacity of polymer-porphyrin binding is 60% higher than that of porphyrin dimerization. The polymer-porphyrin dissociation entropy, $\Delta_{\mathrm{d}}S^{0}_{\mathrm{PL,R}} = (30 \pm 2)\,\mathrm{J\,mol^{-1}K^{-1}}$, was determined from the $\Delta_{\mathrm{d}}H^{0}_{\mathrm{PL,R}}$ and $\Delta_{\mathrm{d}}G^{0}_{\mathrm{PL}}$ values listed in Table 2. The heat capacity values and entropy values show that greater numbers of hydrophobic interactions take place in polymer-porphyrin dissociation

compared to poyphyrin dimer dissociation. This can be explained by considering that both sides of a porphyrin are in contact with water when this molecule is dissociated from a PVP chain; on the other hand, only one extra side of a porphyrin is in contact with water when the dimer is dissociated.

The molecular sizes were examined to further estimate the number of porphyrin binding sites per polymer. The binding segment length of PVP polymer is ~6 nm, assuming that PVP monomer length is ~0.3 nm and there are roughly 20 units per polymer. The diameter of the TPPS is ~2 nm.[5] These values are consistent with PVP chains interacting with both sides of a TPPS molecule.

In Fig. 14B, $R \ln K$ values are plotted as a function of temperature along with the theoretical curve from the Van't Hoff equation. The calculated values of K at 12 °C and 37 °C were 5% and 40%, respectively. These discrepancies are acceptable because of the system and the binding process complexity. Consequently, a 40% error in K relates to a 1 kJ mol^{-1} error in $\Delta_d G^0_{PL}$, which is comparable to errors seen in $\Delta_d H^0_{PL}$ values in ITC.

In order to assess the possibility that TPPS dimers also bind to PVP, a model where both monomer and dimer bind to PVP equally was considered (L, L_2 model). Thus, eq. 16 is modified in the following way:

$$\nu = \frac{n([L]+[L_2])}{K+([L]+[L_2])} \tag{18}$$

where L and L_2 are distinct competing ligands with the exact same binding properties. While the extracted values of $\Delta_d H^0_{PL}$ and n were marginally different by ~5% when using eq. 15, the K values did not correlate to temperature. This means that the Van't Hoff prediction for the L, L_2 model does not correspond to K values.

In summary, our analysis shows that the interaction between TPPS and PVP involves a polymer segment of twenty monomeric units with one porphyrin molecule.

Examination of Absorption Spectra

Normalized absorption spectra in the visible wavelength range for TPPS (Fig. 10) and TPPS-PVP aqueous solutions (Fig. 11) were taken at room temperature. Then, the effects of pH on spectra were examined as PVP concentration increased (Fig. 12). Lastly, the Q and Soret bands were quantitatively examined to evaluate further the binding models of TPPS self-association and TPPS-PVP binding. The values of α and K obtained from ITC experiments were used to extract the actual spectra of TPPS, TPPS dimer, and TPPS-PVP species. These are shown in Figs. 15 & 16.

In Fig. 15, the Q_X bands show an appreciable shift whereas the Q_Y bands do not. When comparing the spectra of the TPPS monomer and dimer, the four Q bands are shifted ~0.04 eV. When comparing the spectra of the bound to unbound TPPS, the two Q_X bands are shifted ~0.03 eV with respect to the monomer. On the other hand, the two Q_Y bands do not show a significant shift. Because the two permanently protonated nitrogens are along the x-axis of the porphyrin by convention[15], the shifts indicate that PVP-TPPS interaction mainly occurs along the x-axis. Thus, this interaction can be attributed to hydrogen bonding between the two x-axis hydrogens of TPPS and the PVP oxygens. The PVP oxygen has two resonance forms, with the form involving the negative charge on the PVP oxygen and a positive charge on the PVP nitrogen engaging in hydrogen bonding (Fig. 9). The π character of this C-N bond favors π-π interactions between polymer and porphyrin.

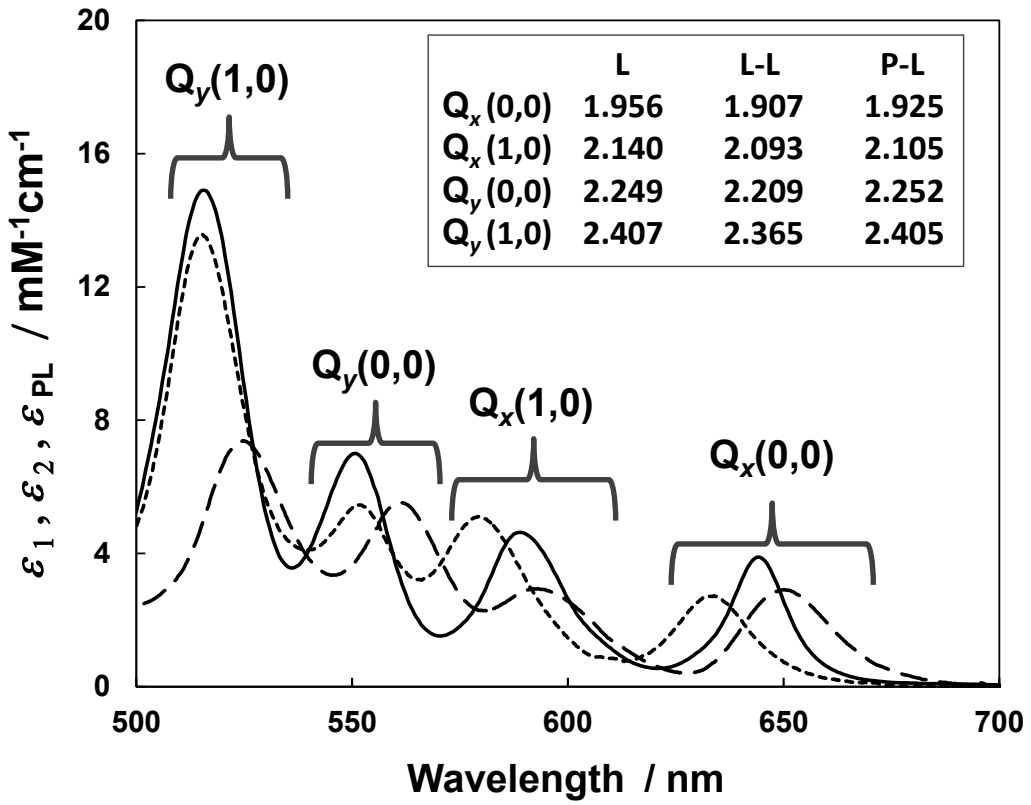

Figure 15 – Normalized absorption spectra for TPPS is shown in the monomeric (short dashed curve, ε_1), dimeric (long dashed curve, ε_2), and bound (solid curve, ε_{PL}) states. The four Q bands, $Q_x(0,0)$, $Q_x(1,0)$, $Q_y(0,0)$ and $Q_y(1,0)$, are shown as well. The inset shows the corresponding transition energy values in eV associated with the bands for the monomer (L), dimer (L-L), and bound (P-L) TPPS.

In Fig. 16, the Soret band shifts to higher wavelengths as PVP concentration increased in TPPS solution. The intensity of these bands is significantly stronger than that of the Q bands so solutions containing low concentrations of TPPS were evaluated. The effect of PVP on the TPPS Soret band included a shift towards higher wavelength, ~0.05 eV. However, the Soret band did not show an appreciable shift as TPPS concentration increased in the absence of PVP. This is qualitatively consistent with the Q_X band shift as seen in Fig. 15.

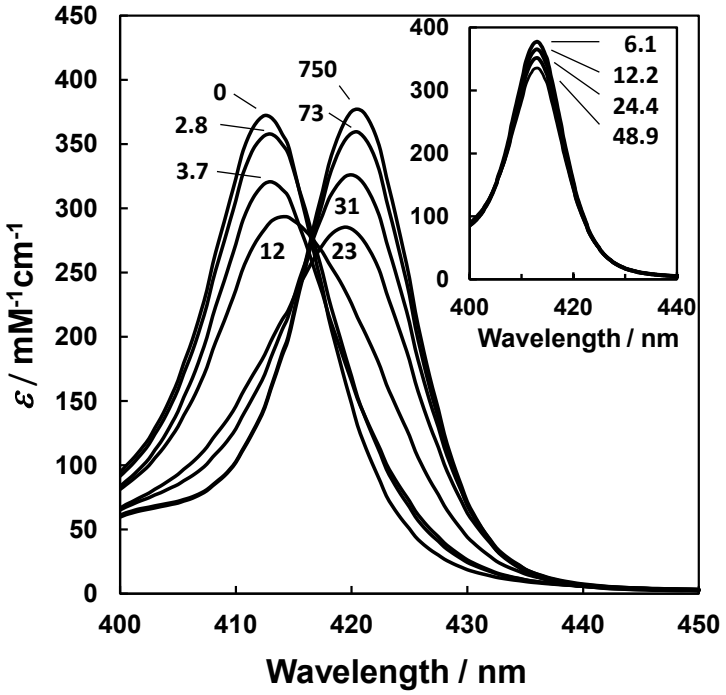

Figure 16 – Normalized absorption spectra for TPPS (sodium phosphate buffer, 10 mM, pH 7.0, 22.5 °C) are shown for TPPS-PVP solutions and TPPS dimerization (see inset). The associated numbers on spectra represent the PVP to TPPS concentration ratio or C_P/C_L. The inset shows spectra for various μM concentrations of TPPS in the absence of PVP.

CONCLUSION

Supramolecular PVP-TPPS structures were formed at TPPS concentrations of 10 μM or higher and examined with absorption spectroscopy and ITC. First, the comparison of experimental values to predicted Van't Hoff behavior showed that TPPS self-association is limited to dimers and that TPPS binds to PVP in the monomeric state. TPPS dimerization and PVP-TPPS binding are both enthalpically driven. However, PVP-TPPS binding is favored with respect to dimerization due to entropic effects. Values of reaction heat capacity are large and reveal the presence of significant hydrophobic interactions. Lastly, the observed spectral shifts in the Q_X, Q_Y, and Soret band region show that the two permanently protonated hydrogens in the porphyrin bind to the PVP oxygen

APPENDIX A

TPPS-PVP Solutions

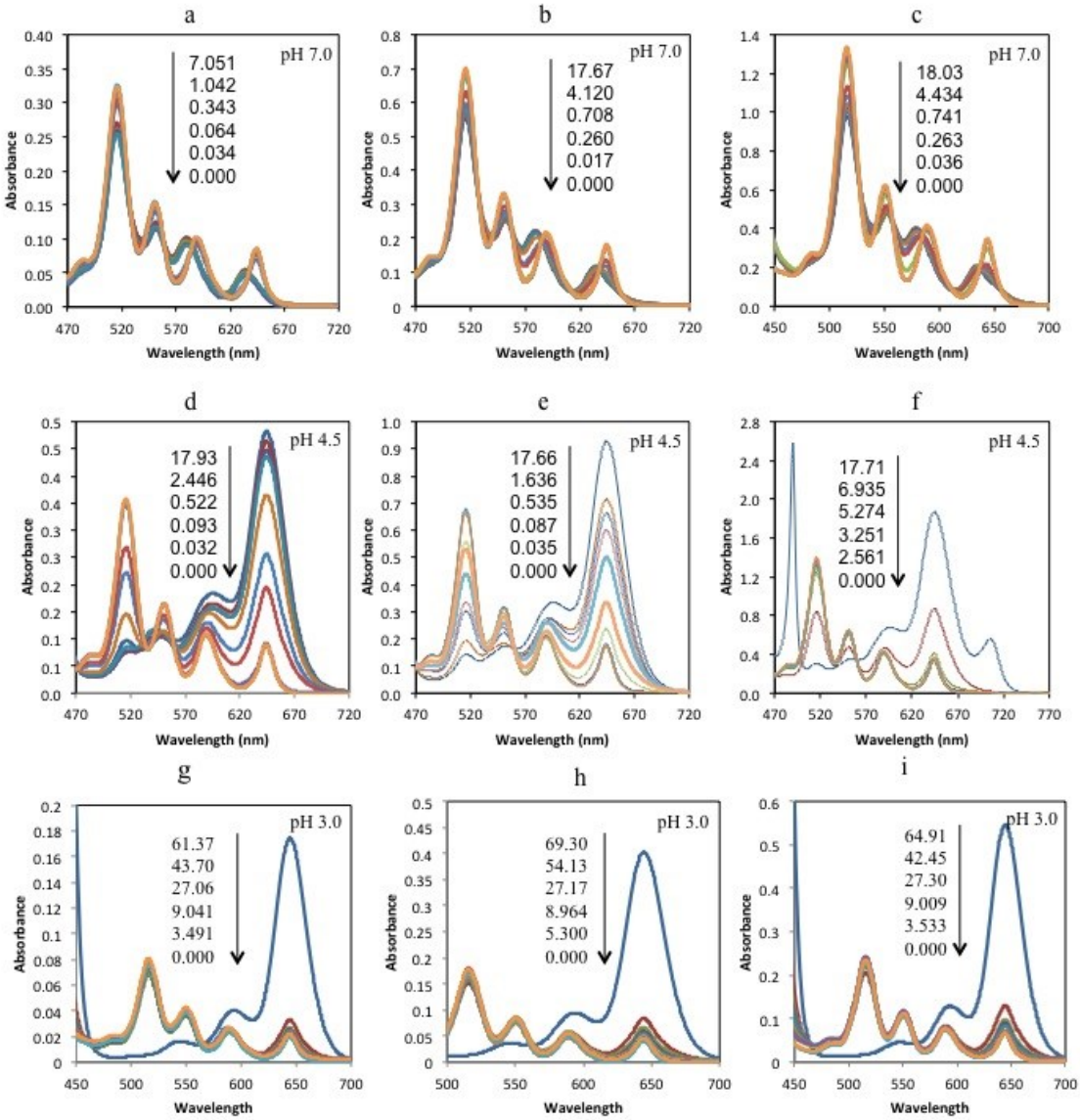

Appendix A – Absorption spectra were taken of TPPS solutions at fixed concentrations. Variable amounts of PVP were added to these solutions at three different pH values: 3.0, 4.5, and 7.0. The pH of individual solutions is listed on each spectrum. The values listed with the arrow indicate the decreasing millimolar concentrations of PVP. The concentrations of TPPS are as follows: a) 0.025 mM; b) 0.050 mM; c) 0.100 mM; d) 0.025 mM; e) 0.050 mM; f) 0.100 mM; g) 0.025 mM; h) 0.050 mM; i) 0.100 mM. As PVP concentration increased, spectra approached a common spectral curve.

REFERENCES

1. Ethirajan, M.; Chen, P.; Joshi, P.; Pandey, R.K. The role of porphyrin chemistry in tumor imaging and photodynamic therapy. *Chem. Soc. Rev.* **2011**, *40*, 340-362.
2. Xing, C.; Xu, Q.; Tang, H.; Liu, L.; Wang, S. Conjugated Polymer/Porphyrin Complexes for Efficient Energy Transfer and Improving Light-Activated Antibacterial Therapy. *J. Am. Chem. Soc.* **2009**, *131*, 13117-13124.
3. Arai, Y.; Segawa, H. J-Aggregation of protonated *meso*-tetrakis(sulfonatothienyl)porphyrin isomers: Morphological selection of self-assembled nanostructures from structurally similar zwitterionic porphyrins. *Chem. Commun.* **2010**, *46*, 4279-4281.
4. Lu, X; Zhang, X.P. Catalytic C-H functionalization by metalloporphyrins: recent developments and future directions. *Chem. Soc. Rev* **2011**, *40*, 1899-1909.
5. da Costa, V.C.P.; Ribiero, A.C.F.; Sobral, A.J.F.N.; Lobo, V.M.M.; Annunziata, O.; Santos, C.I.A.V. Mutual and self-diffusion of charged porphyrines in aqueous solutions. *J. Chem. Thermodyn*. **2012**, *47*, 312-319.
6. Zhang, L.; Liu, M. *J. Phys. Chem. B.* **2009**, *113*, 14015-14020.
7. Chandreshekar, T.K.; van Willigen, H.; Ebersole, M.H. Optical and Electron Spin Resonance Study of Cation and Cation-Crown Ether Induced Dimerization of Tetrakis(4-sulfonatophenyl)porphyrin. *J. Phys. Chem*. **2984**, *88*, 4326-4332.
8. Andrade, S.; Teixeria, R.; Costa, S.M.B.; Sobral, A.J.F.N. Self-aggregation of free base porphyrins in aqueous solution and in DMPC vesicles. *Biophys. Chem.* **2008**, *133*, 1-10.
9. Aggarwal, L.P.F.; Borissevitch, I.E. On the dynamics of the TPPS4 aggregation in aqueous solutions: successive formation of H and J aggregates. *Spectrochim. Acta. A. Mol. Biomol. Spectrosc.* **2006**, *63*, 227-223.
10. Dutta, P.; Rai, R.; Pandey, S. Effect of ionic liquid on J-aggregation of meso-tetrakis(4-sulfonatophenyl)porphyrin within aqueous mixtures of poly(ethylene glycol). *J. Phys. Chem. B.* **2011**, *115*, 3578–3587.
11. Synytsya, A.; Blafkova, P.; Volka, K.; Král, V. Interaction of meso-tetrakis(4-sulphonatophenyl)porphine with chitosan in aqueous solutions. *Spectrochim. Acta. A. Mol. Biomol. Spectrosc.* **2007**, *66*, 225–235.
12. Lee, Y.; Baron, E.D. Photodynamic Therapy: Current Evidence and Applications in Dermatology. *Semin. Cutan. Med. Surg.* **2011**, *30*, 199-209.
13. Hollingsworth, J.V.; Richard, A.J.; Vicente, M.G.H.; Russo, P.S. Characterization of the self-assembly of meso-tetra(4-sulfonatophenyl)porphyrin (H_2TPPS^{4-}) in aqueous solutions. *Biomacromolecules*, **2012**, *13*, 60-72.
14. da Costa, V.C.P.; Hwang, B.J.; Eggen, S.E.; Wallace, M.J.; Annunziata, O. Formation and thermodynamic stability of polymer-porphyrin supramolecular structures in aqueous solutions, *J. Chem. Thermodynamics*, in press.

15. Hashimoto, T.; Choe, Y.K.; Nakano, H.; Hirao, K. Theoretical Study of the Q and B Bands of Free-Base, Magnesium, and Zinc Porphyrins, and Their Derivatives. *J. Phys. Chem. A* **1999,** *103*, 1894–1904.
16. Castriciano, M.A.; Romeo, A.; De Luca, G.; Villari, V.; Scolaro, L.M.; Micali, N. Scaling the chirality in porphyrin J-nanoaggregates. *J. Am. Chem. Soc.* **2011**, *133*, 765–767.
17. Gharib, F.; Soleimani, R.; Farajtabar, A.; Aghaei, H. Complexation of 5,10,15,20-Tetrakis(4-sulfonatophenyl)porphyrin with the Cadmium(II) Ion at Different Ionic Strengths. *J. Chem. Eng. Data* **2009**, *54*, 2060-2066.
18. Egawa, Y.; Hayashida, R.; Anzai, J. pH-Induced Interconversion between J-Aggregates and H-Aggregates of 5,10,15,20-Tetrakis(4-sulfonatophenyl)porphyrin in Polyelectrolyte Multilayer Films. *Langmuir* **2007**, *23*, 13146–13150.
19. Kadajji, V.G.; Betageri, G.V. Water Soluble Polymers for Pharmaceutical Applications. *Polymers* **2011**, *3*, 1972-2009.
20. Ladbury, J.E.; Klebe, G.; Freire, E. Adding calorimetric data to decision making in lead discovery: a hot tip. *Nat. Rev. Drug Discov.* **2010**, *9*, 23-28.
21. Chaires, J. Calorimetry and Thermodynamics in Drug Design. *Annu. Rev. Biophys.* **2008**, *37*, 135-151.
22. Pasternack, R.F.; Huber, P.R.; Boyd, P.; Engasser, G.; Francesconi, L.; Gibbs, E. On the Aggregation of Meso-Substituted Water-Soluble Porphyrins. *J. Am. Chem. Soc*. **1972**, *94*, 4511-4517.
23. Martin, R.B. Comparisons of Indefinite Self-Association Models. *Chem. Soc. Rev.* **1996**, *96*, 3043-3064.
24. Yu, Y.B.; Privalov, P.L.; Hodges, R.S. Contribution of Translational and Rotational Motions to Molecular Association in Aqueous Solution. *Biophys. J.* **2001**, *81*, 1632-1642.
25. van Holde, K.E. *Physical Biochemistry*, 2nd ed.; Prentice-Hall: Englewood Cliffs, NJ, 1985.
26. Sadeghi, R.; Zafarani-Moattar, M.T. Thermodynamics of aqueous solutions of polyvinylpyrrolidone. *J. Chem. Thermodyn.* **2004**, *36*, 665-670.